Characterization and Magnetic Resonance Imaging of a Rat Model of Human B-Cell Central Nervous System Lymphoma

Carole Soussain,[1] Leslie L. Muldoon,[1,2] Csanad Varallyay,[1] Kristoph Jahnke,[1,3] Luciana DePaula,[4] and Edward A. Neuwelt[1,5,6]

Abstract

Purpose: The incidence of primary central nervous system lymphoma (PCNSL) is increasing. Therapeutic approaches remain controversial. An animal model that mimics the clinical situation would be useful for evaluating PCNSL biology and treatment.

Experimental Design: Nude rats received intracerebral (caudate nucleus, $n = 49$) or intraventricular ($n = 4$) inoculation of human B-lymphoma cell line MC116. Two to five weeks after tumor inoculation, magnetic resonance imaging (MRI) was done ($n = 24$), and rat brains were assessed for pathology. Five rats each received whole-brain radiotherapy (WBRT, 20 Gy) or high-dose i.v. methotrexate (3 g/m^2).

Results: Intracerebral tumors developed in 84% of evaluable animals with no pretreatment, 79% of rats pretreated with 4 Gy total body irradiation, and 92% of rats pretreated with cyclophosphamide (300 mg/m^2). MRI showed abnormal T2 signal and gadolinium enhancement on T1-weighted images, consistent with tumor growth 19 to 24 days after inoculation. Tumor cells staining positively for B-lymphoma markers infiltrated within the inoculated hemisphere, along fiber tracks to the contralateral hemisphere, and along the subarachnoid space and ventricles. Tumors showed reactive gliosis. Intraventricular tumor cell injection resulted in periventricular parenchymal infiltration in both hemispheres. Radiation and methotrexate were effective *in vitro*, but only WBRT was clearly effective after 1 week in the intracerebral model.

Conclusion: This model closely mimics human PCNSL in terms of imaging, histology, and treatment sensitivity and will be useful for the development of future therapeutic strategies for PCNSL.

Primary central nervous system lymphoma (PCNSL) is a rare disease, but its incidence has increased in immunocompetent people over the last three decades at a rate greater than the increase in systemic lymphoma (1). PCNSL has a characteristic pattern of diffuse and perivascular infiltration (2, 3). More than 90% of PCNSL are diffuse large B-cell lymphomas (4, 5), but they have a worse prognosis than systemic B-cell lymphoma. Despite a large number of clinical studies, therapy for PCNSL remains controversial (3, 6–9). Unlike other primary CNS tumors, the course of the disease is unaffected by surgery due to the highly infiltrative nature of the tumor cells. PCNSL is radiosensitive but not curable by radiotherapy alone (6). Similarly, PCNSL is chemosensitive, but chemotherapeutics used in systemic diffuse large B-cell lymphomas (e.g., the standard "CHOP" regimen of cyclophosphamide, doxorubicin, vincristine, and prednisone) are ineffective (10). Chemoresistance is due at least in part to the blood-brain barrier (BBB) that limits the penetration of chemotherapy from the blood into the tumor (9, 11, 12). Although current therapies have high rates of recurrence and treatment-induced neurotoxicity, the standard of care for PCNSL remains high-dose systemic methotrexate, with or without whole-brain radiotherapy (WBRT; refs. 3, 6, 7, 13).

An animal model that closely mimics the clinical situation would be useful for evaluating PCNSL biology and new treatment approaches. Previously, animal models of leptomeningeal lymphoma and brain lymphoma have been done with T-cell lines in the majority of cases (14–16). One xenograft model of CNSL was conducted with human B-lymphoma cells, but focused only on the pathologic results (17). Here, we report two xenograft models of CNSL (intraventricular and intracerebral), including pathologic and radiographic characterization. Pilot studies were done to show that the model accurately mimics the clinical responses to radiotherapy and high-dose methotrexate.

Authors' Affiliations: Departments of [1]Neurology, [2]Cell and Developmental Biology, [3]Medicine, [4]Radiation Oncology, and [5]Neurosurgery, Oregon Health & Science University, and [6]Veterans Administration Medical Center, Portland, Oregon
Received 9/28/06; revised 12/12/06; accepted 2/2/07.

Grant support: Veteran's Administration Merit Review Grant and NIH grants NS33618, NS34608, and NS44687 from the National Institute of Neurological Disorders and Stroke to E.A. Neuwelt and by a Roche Foundation for Anemia Research grant to C. Soussain.

The costs of publication of this article were defrayed in part by the payment of page charges. This article must therefore be hereby marked *advertisement* in accordance with 18 U.S.C. Section 1734 solely to indicate this fact.

Note: Current address for C. Soussain: Centre René Huguenin, Service d'Hématologie, Saint-Cloud, France.

Requests for reprints: Edward A. Neuwelt, Blood-Brain Barrier and Neuro-Oncology Program, Department of Neurology, Oregon Health and Science University, 3181 Sam Jackson Park Road, L603, Portland, OR 97239-3098. Phone: 503-494-5626; Fax: 503-494-5627; E-mail: neuwelte@ohsu.edu.

doi:10.1158/1078-0432.CCR-06-2379

Materials and Methods

Tissue culture. MC116 human B-cell lymphoma cells (EBV and HIV negative; from the American Type Culture Collection, Manassas, VA) were cultured in suspension in RPMI 1640 supplemented with 20% fetal bovine serum, 2 mmol/L L-glutamine, 10 mmol/L HEPES buffer, and antibiotics. Cells were harvested immediately before intracerebral implantation and were used only if viability exceeded 80%. For *in vitro* analysis of toxicity, cells were plated in 12-well tissue culture plates and treated either with methotrexate (doses 0.01-100 μmol/L for 3 days) or irradiated in a cesium irradiator (1-10 Gy). Toxicity was assessed by trypan blue exclusion in duplicate samples.

Tumor inoculation. The care and use of animals were approved by the Institutional Animal Care and Use Committee and were supervised by the Oregon Health & Science University (OHSU) Department of Animal Care. In the initial study, female athymic nude rats (*rnu/rnu*, 200-220 g, from the OHSU Blood-Brain Barrier Program in-house colony) were treated with (n = 18) or without (n = 22) total body irradiation (TBI) 24 h before tumor inoculation. Animals were anesthetized with i.p. ketamine (60 mg/kg) and i.p. diazepam (7.5 mg/kg), then irradiated with 4 Gy in a cesium irradiator the day before cell inoculation. In the second study, 13 rats were treated with cyclophosphamide (300 mg/m^2 i.v.) 24 h before tumor implantation.

For tumor implantation, rats were anesthetized with i.p. ketamine (60 mg/kg) and i.p. diazepam (7.5 mg/kg). Animals' heads were held in a stereotactic device, a midsagittal incision was done, and a 2-mm burr hole drilled in the skull. Animals received 1.2 to 1.5 $\times$ 10^6 of >80% viable MC116 cells in a volume of 12 to 15 μL over 5 min using a 27 gauge needle. For intracerebral inoculation (n = 36 in the initial study; n = 13 in the second study), cells were stereotactically injected in the right caudate putamen (vertical, bregma 6 mm; lateral, bregma 3.1 mm). The needle was initially advanced to a depth of 7 mm and then withdrawn to a depth of 6 mm to limit reflux up the needle track. For intraventricular injection (n = 4), the coordinates were vertical, 4.0 mm; lateral, 1.4 mm. Three rats (two intracerebral, one intraventricular) showed reflux of cell infusate at the injection site. After inoculation, the needle was slowly removed, and the skin incision was closed. The animals were examined daily and weighed biweekly for 2 to 5 weeks after tumor implantation, then daily after treatment. Animals were sacrificed if they showed severe clinical signs or symptoms or >20% weight loss.

In study 1, four intracerebral rats (two with TBI, two without TBI) and two intraventricular rats were initially followed for clinical symptoms and pathology. Day 19 after implantation was chosen for baseline imaging and treatment to allow 7 days before emergence of clinical symptoms for serial imaging and tumor therapy. Three animals in this study were not evaluable due to technical issues. In the second study, rats pretreated with cyclophosphamide were used only for tumor volumetrics at day 26 (n = 10), or tissues were harvested on day 19 for pathology. Brain, spleen, liver, and cervical and abdominal lymph nodes were assessed for the presence of lymphoma by ARUP Laboratories (Salt Lake City, UT).

Magnetic resonance imaging. Imaging was done 2 to 5 weeks after tumor implantation. A total of 24 rats were imaged: 12 were scanned once, 3 were scanned twice to thrice to determine the onset of visible tumor, and 9 were scanned twice in the therapy study. Five rats were not imaged due to technical issues. Rats were anesthetized with i.p. ketamine (60 mg/kg) and i.p. diazepam (7.5 mg/kg) and imaged on a 3T MR scanner (Siemens Magnetom Trio, Erlangen, Germany) using a custom rat head transmitter-receiver coil. The 3T imaging sequences were T1 spin echo (SE) with relaxation time (TR) = 750 ms and echo time (TE) = 12 ms; T2 turbo spin echo (TSE; TR, 5,430 ms; TE, 78 ms); and fluid-attenuated inversion recovery (FLAIR; TR, 9280 ms; TE, 89 ms; inversion time, 2,100 ms). The voxel size was 0.26 $\times$ 0.26 $\times$ 2 mm for coronal scans. T1 scans were done before and after gadolinium (Omniscan, Amersham Health AS, Oslo, Norway) at a dose of 0.1 to 0.3 mmol/kg injected into a femoral vein. In some animals, serial MR scans were done on days 14 to 30 to assess tumor growth.

Pilot treatment studies. Two nonrandomized pilot studies of treatment response were done on day 19, immediately after confirmation of the presence of tumor on FLAIR MR images. WBRT was done in the Department of Radiation Oncology at OHSU. Shielding blocks were designed to protect the eyes, oropharynx, and salivary glands from radiation toxicity. The animals (n = 5, including two with prior TBI) were anesthetized with i.p. ketamine (60 mg/kg) and i.p. diazepam (7.5 mg/kg). A single fraction of 20 Gy was delivered using a single 6-MV photon beam with tissue-equivalent material to ensure dose homogeneity throughout the whole brain. In rats, 20 Gy WBRT has been shown to simulate 60 Gy of fractionated radiation in the Hopewell model (18). For the chemotherapy study, methotrexate (3 g/m^2) was injected i.v. into the femoral vein in isofluorane-anesthetized rats (n = 5, no pretreatment). Folinic acid (Leucovorin, 10 mg) was given i.p. twice a day for 3 days starting 24 h after methotrexate. A second magnetic resonance scan was done in treated animals 1 week after treatment (day 26).

Histology. Rats were sacrificed at different time points (days 19 to 44 or when symptoms indicated) after inoculation using intracardiac thiopental injection. Brains were excised and fixed in 10% buffered formalin for vibratome sectioning, 100 μm in the coronal plane. Sections were stained with either hematoxylin or H&E. Immunohistochemistry was done using indirect immunoperoxidase labeling, with primary antibody reacted with biotinylated protein A followed by avidin and biotinylated peroxidase (Vectastain ABC kit, Vector Labs, Burlingame, CA). Brown reaction products were formed with diaminobenzidine. All antibodies were from Santa Cruz Biotechnology (Santa Cruz, CA) except CD22, which was from Chemicon International Inc. (Temecula, CA). Immunostaining included pan-leukocyte marker CD45 (sc-1187), B-cell markers CD20 (sc-7733), and CD22 (CBL533), anti-CD30 (sc-1737), glial cell marker GFAP (sc-33673), antiapoptotic factor bcl-2 (sc-492), and natural killer (NK) cell marker NK-p43 (sc-18161). For tumor volumetrics, every sixth brain section was stained with hematoxylin, then imaged at high resolution (30 μm pixel diameter) on an Epson 1640XL flatbed scanner using Adobe Photoshop software. Tumor volume was assessed using NIH Image software.

Results

MRI of the intracerebral CNSL model. Magnetic resonance imaging (MRI) was done on 24 nude rats following intracerebral implantation of MC116 human B-lymphoma cells. A total of 39 scans were done at time points ranging from 14 to 32 days after tumor implantation. In very large tumors (>100 mm^3, n = 3), MRI showed T2/FLAIR signal changes and gadolinium enhancement at the inoculation site (caudate nucleus) and in the cortex and ventricles at 19 to 24 days after implantation (Fig. 1). High signal intensity on FLAIR images indicates tumor infiltration and edema throughout the inoculated hemisphere and also in the contralateral side along white matter tracts (Fig. 1A). With our parameters, pregadolinium T1-weighted images showed diffuse slightly elevated signal intensity in the injected hemisphere in large tumors (Fig. 1B). Gadolinium enhancement was found primarily in the central region of the tumor (Fig. 1C). Mass effect with midline shift to the left and ventricle compression was present in most of the animals. In smaller tumors (2.6-33.7 mm^3, n = 15), FLAIR sequences seemed to be the most sensitive in the delineation of the tumor-infiltrated brain. A good visual correlation between MRI and hematoxylin staining was observed (Fig. 1D).

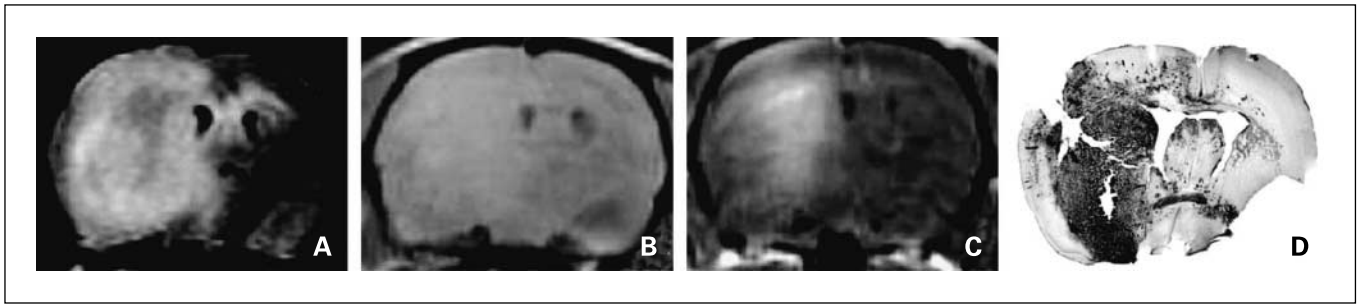

Fig. 1. MRI of intracerebral CNSL model. Nude rats received 1.2 to 1.5 $\times$ 10^6 MC116 cells inoculated in the right caudate nucleus. *A* to *D,* MRI and histology at day 26 after implantation in a rat with a large CNSL tumor. *A,* FLAIR. *B,* T1-weighted. *C,* T1 with gadolinium. *D,* histology with hematoxylin (original magnification, $\times$3).

Histology and immunohistochemistry of the intracerebral CNSL model. In the initial study, tumor growth was detected by histology and/or MR in 27 of 33 evaluable animals (82%), and tumors ranged in size from tiny (2 mm^3) to huge (175 mm^3) at 19 to 26 days after tumor implantation (Table 1). Animals were judged negative for tumor only if no positive immunohistochemistry for B-cell markers was detected along the needle track. The consistency of tumor growth and the variability of tumor volumes was of concern. We first evaluated the effect of low-dose TBI (4 Gy 24 h before tumor implantation) to reduce the population of antitumoral NK cells that could potentially decrease the success rate of the tumor inoculations. TBI did not seem to impact either the percentage of animals growing intracerebral tumors or the size of the tumor at 19 to 26 days after implantation (Table 1). A second study was done using cyclophosphamide pretreatment (300 mg/m^2 24 h before tumor implantation) to decrease innate immunity. Brain tumors were detected in 12 of 13 animals, and all nine untreated control animals had moderately sized tumors (33 $\pm$ 16.9 mm^3, mean $\pm$ SD) at 26 days after implantation, with no tiny or giant outliers (Table 1). Rats with tumors showed no neurologic symptoms and never lost more than 10% of their baseline body weight before day 19. Animals with large intracerebral CNSL lost about 10% of body weight between days 19 and 26. Three animals evaluated at day 19 after tumor implantation showed no evidence of systemic lymphoma.

Immunohistochemistry was used to evaluate tumor growth pattern and brain infiltration. All positive animals showed tumor at the injection site within the caudate nucleus (Fig. 2A) and diffuse infiltration of the MC116 cells into the cortex. The tumors were not well demarcated. Necrotic tumor was observed in the central areas of tumor inoculation in six animals with large tumors, but not in infiltrated brain. Rats with medium- to large-size tumors showed tumor tracking along the corpus callosum into the contralateral hemisphere (Fig. 2B). In some animals, tumor was found lining the ventricles (Fig. 2C) and in the meninges in the subarachnoid space. Perivascular infiltration was also a typical feature of this lymphoma model (Fig. 2D). Infiltrating individual cells and tumor nodules showed surface immunostaining for human CD45, CD20, and CD22 (Fig. 2). Normal rat brain was negative for CD45, CD20, and CD22 staining (data not shown). Tumors and normal rat brains were nonreactive for CD30, a marker of activated cells that can be useful in the diagnosis of Hodgkin lymphoma.

Further immunostaining was done to assess CNSL tumor biology. Figure 3 shows hematoxylin (Fig. 3A) and CD20 (Fig. 3B) staining in a medium-size tumor in an animal pretreated with cyclophosphamide. Tumors were negative for bcl-2 (data not shown). Staining for NK cells showed diffuse immunoreactivity in the central area of the tumors (Fig. 3C), but no clearly defined cells were visible. GFAP staining showed diffuse reactive gliosis within the brain tumor and 1 to 2 mm surrounding the tumor (Fig. 3D). GFAP-positive cells were often located adjacent to tumor cells (Fig. 3E).

Pilot tests of therapeutic approaches. MC116 cells were sensitive to both methotrexate and radiation *in vitro*. A 3-day treatment with methotrexate killed the cells at concentrations above 0.03 μmol/L as determined by trypan blue exclusion (Fig. 4A). Cells treated with radiation showed toxicity at 2 to 10 Gy on days 3 and 4 after treatment (Fig. 4B). Growth rates and viability of cells treated with low dose radiation (2 to 3 Gy) recovered to control levels by 7 days, but cells did not recover from the highest radiation dose tested (Fig. 4B).

Five rats with MRI-confirmed tumor received one dose of i.v. methotrexate (3 g/m^2) on day 19 immediately after MR,

Table 1. Consistency of tumor growth

Treatment	All evaluable rats		Untreated controls			
	Number tested	Tumor, *n* (%)	Large tumor	Medium tumor	Small tumor	Volume (mm^3)
None	19	16 (84)	2	2	4	48.4 $\pm$ 66.2
Total body irradiation	14	11 (79)	2	5	2	54.8 $\pm$ 63.4
Cyclophosphamide	13	12 (92)	0	9	0	33.3 $\pm$ 16.9

NOTE: Total body irradiation consisted of 4 Gy 24 h before tumor inoculation. Cyclophosphamide treatment consisted of 300 mg/m^2 24 h before tumor inoculation.

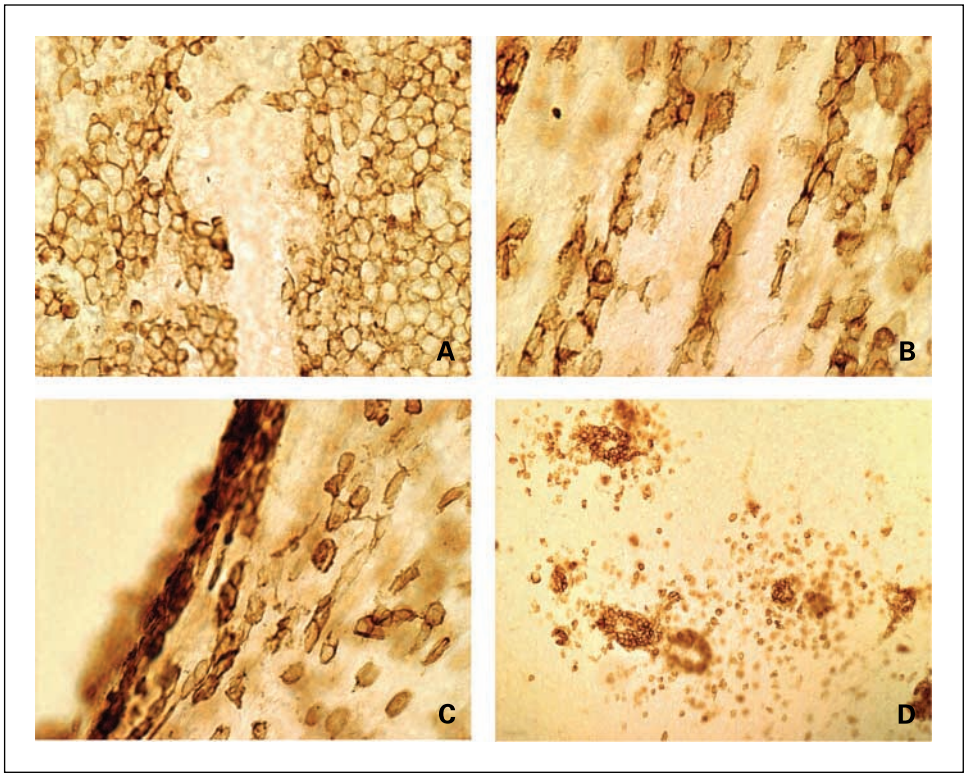

Fig. 2. Immunohistochemistry of intracerebral CNSL growth. The brain from a rat with a large diffusely infiltrative intracerebral tumor was histologically assessed 21 d after tumor inoculation. *A,* CD45 staining at the inoculation site (original magnification, ×200). *B,* CD20 staining in the fiber tracks of the corpus callosum (original magnification, ×200). *C,* CD45 staining along the ventricle in the left hemisphere (original magnification, ×200). *D,* CD22 staining in cortex 4 mm from injection site showing perivascular infiltration (original magnification, ×50).

followed by 3 days of leucovorin rescue. Follow-up MRI scans were obtained on day 26, except in one rat with severe neurologic symptoms that was sacrificed on day 25. An increase in area of enhancement was seen in three animals on both T2 (Fig. 5A) and T1 + gadolinium images (Fig. 5B), whereas no change in enhancement was detected in the final animal. Histology showed infiltrative tumor in all five animals (Fig. 5C), with a mean tumor volume of 17.7 ± 9.7 mm^3

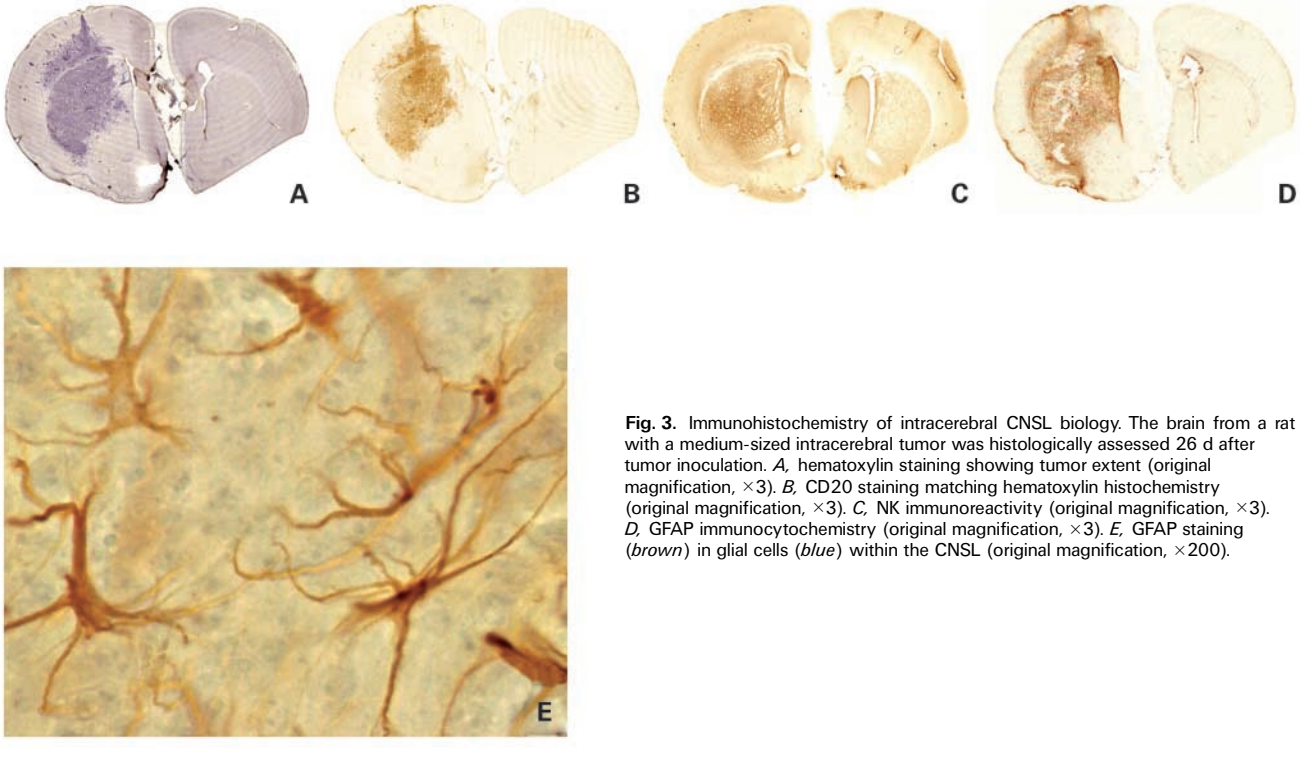

Fig. 3. Immunohistochemistry of intracerebral CNSL biology. The brain from a rat with a medium-sized intracerebral tumor was histologically assessed 26 d after tumor inoculation. *A,* hematoxylin staining showing tumor extent (original magnification, ×3). *B,* CD20 staining matching hematoxylin histochemistry (original magnification, ×3). *C,* NK immunoreactivity (original magnification, ×3). *D,* GFAP immunocytochemistry (original magnification, ×3). *E,* GFAP staining (*brown*) in glial cells (*blue*) within the CNSL (original magnification, ×200).

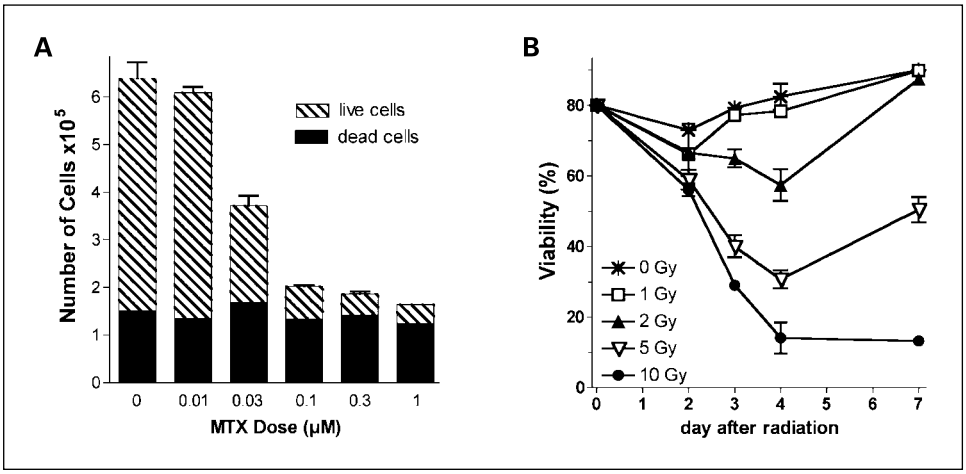

Fig. 4. *In vitro* cytotoxicity of methotrexate and radiation in MC116 cells. *A,* exponentially growing MC116 cells were treated with methotrexate at the indicated doses. Cell number and viability were determined by trypan blue exclusion after 3 d of continuous incubation with the drug. *B,* exponentially growing MC116 cells were treated with the indicated radiation dose in a cesium irradiator, then plated in six-well culture dishes. Cell number and viability were determined by trypan blue exclusion 2, 3, 4, and 7 d after treatment. Points, mean and range of two measurements.

(n = 5). CD45 immunohistochemistry showed clusters of tumor cells throughout the inoculated hemisphere (Fig. 5D).

Five animals with MRI-confirmed tumor were treated with a single dose of WBRT (20 Gy) on day 19 immediately after MR. FLAIR MRI 7 days after radiation treatment showed increased signal enhancement within the tumor, but no change in volume compared with pretreatment scans (Fig. 6A). T1-weighted images showed reduced diffuse high signal intensity and a change in the area of gadolinium enhancement (Fig. 6B). Histochemistry showed minimal tumor (<1 mm^3) in three rats and small tumor (3.9 and 5.2 mm^3) in two animals by hematoxylin staining (Fig. 6C). All five rats had scattered CD45-positive staining in enlarged and necrotic cells near the inoculation site (Fig. 6D).

Intraventricular CNSL model. Lymphoma cells were inoculated into the right ventricle after TBI (4 Gy) in four rats. All four animals showed tumor growth. These rats showed behavioral changes such as agitation in response to noise around day 17 after inoculation, and a weight loss of ≥10% of baseline body weight occurred between days 14 and 17.

After intraventricular injection, FLAIR MRI showed large ventricles with periventricular tumor manifestations (Fig. 7A and B). Gadolinium-enhanced T1 images (data not shown) did not show significant enhancement. Immunocytochemistry for CD20 showed diffuse tumor cell infiltration into the rat brain along the needle track (Fig. 7C). Diffuse tumor infiltration was observed around both the right and left ventricles (Fig. 8A), and tumor cells along the meninges partially infiltrated into the parenchyma (Fig. 8B).

Discussion

The investigation of CNS lymphoma biology, pathophysiology, pathology, and treatment response has been difficult in patients due to the rarity of the disorder and in animals due to the lack of appropriate models. PCNSL cannot be studied adequately using *in vitro* models, and data concerning systemic lymphomas cannot be extrapolated to brain lymphomas. Few studies of animal models of PCNSL have been reported (14–17). We report the development of an intracerebral and an intraventricular CNSL model in the nude rat that closely mimic clinical PCNSL.

No cell line derived from human PCNSL is commercially available. We chose the MC116 human B-cell lymphoma cell line for this study because it was previously assessed for pathology in the brain (17). Although MC116 cells have been

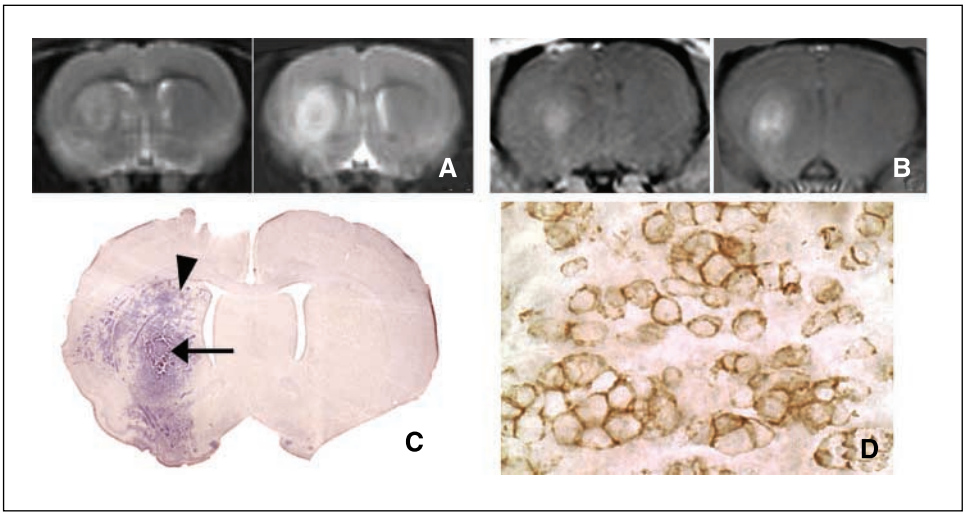

Fig. 5. Effect of high-dose methotrexate in rat CNSL. Rats with intracerebral MC116 tumors were treated with one dose of i.v. methotrexate (3 g/m^2, n = 5) on day 19 after implantation. *A,* T2 MR sequences before (*left*) and 1 wk after (*right*) treatment. *B,* T1 with gadolinium before (*left*) and 1 wk after (*right*) treatment. *C,* hematoxylin staining on day 26 (magnification, ×3). Arrow, inoculation site; arrowhead, site for CD45 immunohistochemistry (*D*; original magnification, ×200).

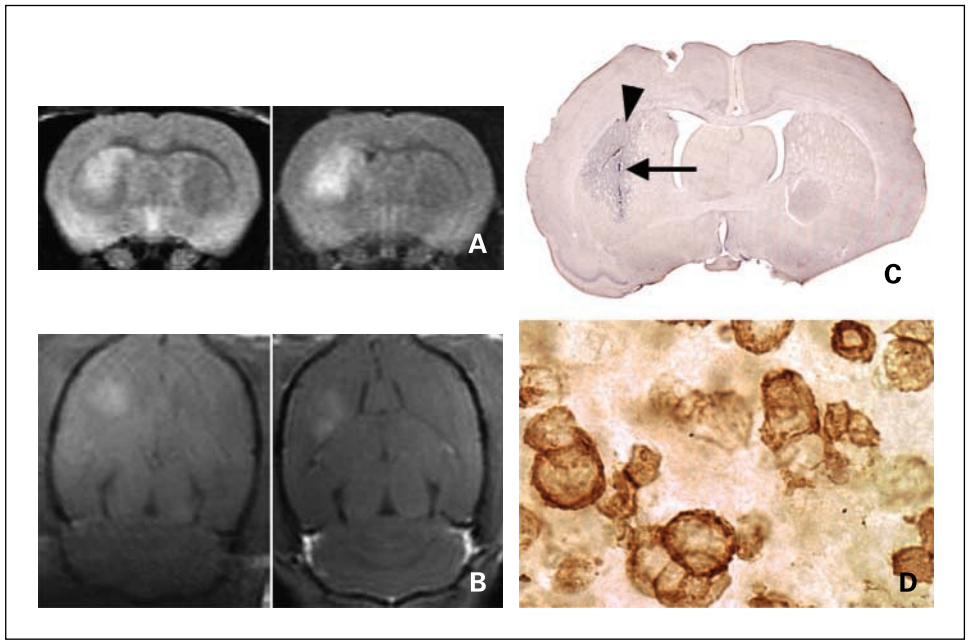

Fig. 6. Effect of WBRT in rat CNSL. Rats with intracerebral MC116 tumors were treated with cranial irradiation (20 Gy, $n = 5$) on day 19 after implantation. *A,* FLAIR MR sequences before (*left*) and 1 wk after (*right*) treatment. *B,* T1 with gadolinium in the horizontal plane before (*left*) and 1 wk after (*right*) treatment. *C,* hematoxylin staining on day 26 (magnification, ×3). Arrow, inoculation site; arrowhead, site for CD45 immunohistochemistry (*D*; original magnification, ×200). Unlike the FLAIR images, gadolinium-enhanced images and histology show tumor response.

reported to express bcl-2 (19), we did not detect this by Western blot or immunostaining in exponentially growing cells, in comparison to positive staining in another human tumor cell line. Sections from three untreated control animals showed no bcl-2 immunostaining above background. Tumors were positive for B-cell markers CD20 and CD22 and pan-leukocyte marker CD45, but negative for CD30, matching the usual clinical immunoreactivity (3, 20).

CNSL tumor growth was inconsistent in the first study, independent of prior TBI. The consistency of tumor take and tumor size was improved by pretreatment with cyclophosphamide, similar to the effect shown for models of CNS gene therapy (21). The pathologic pattern of brain infiltration mimics human PCNSL, with a diffuse and perivascular growth pattern in the cortex, ventricles, and subarachnoid space. Tumor can be visualized on MRI before animals show clinical symptoms of disease, but signal intensity changes are variable, similar to human disease (22). The survival time is long enough to allow the evaluation of therapeutic procedures.

The standard of care for PCNSL is high-dose systemic methotrexate, with or without WBRT (3, 6, 7, 13). The human B-lymphoma cells used in these studies were sensitive to both methotrexate and radiation *in vitro*. In rats treated with a single i.v. dose of methotrexate with leucovorin rescue, MRI showed both increased signal intensity and an increase in the volume of brain showing signal enhancement. Histology showed the presence of viable tumor infiltrated into brain parenchyma. Human PCNSL show variable sensitivity to methotrexate-based chemotherapies with a complete remission rates ranging from 30% to 50% in various studies after multiple courses of chemotherapy (23–26). Many factors could be responsible for the lack of methotrexate response in our pilot *in vivo* study, including the pharmacology of methotrexate or leucovorin rescue (27, 28) or the short time frame of the pilot study. Delivery of agents across the BBB and brain-tumor barrier is a major issue limiting the efficacy of chemotherapeutic approaches to brain tumor therapy (9, 12). PCNSL permeability is variable in humans as well as in the rat models, as indicated by the focal areas of gadolinium enhancement on MRI that were smaller than the extent of the tumor seen on FLAIR sequences. Methotrexate may only penetrate into the central area of the tumor with a somewhat leaky BBB.

The pilot *in vivo* study of radiotherapy used the Hopewell model of 20 Gy to simulate 60 Gy of fractionated radiation (18). MRI showed no reduction in area of enhancement on FLAIR 1 week after WBRT. Gadolinium enhancement on T1-weighted images showed changes but not necessarily shrinkage. Pathology and immunohistochemistry showed minimal tumor volumes and scattered CD20-positive cells. Thus, radiotherapy seemed to be effective in this model, sharing a key feature with human PCNSL that is exquisitely radiosensitive. Human PCNSL is not curable by WBRT alone (8). Because of the short

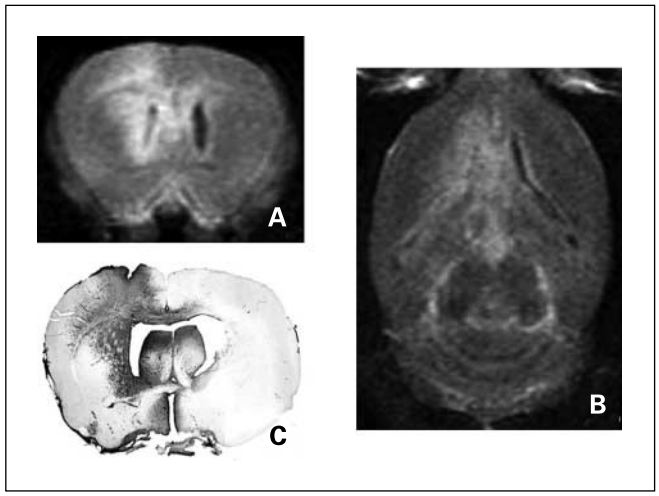

Fig. 7. Intraventricular CNSL model. Nude rats were pre-irradiated with 4 Gy TBI, followed by inoculation of 1.2 to 1.5 × 10^6 MC116 cells into the right ventricle. *A,* FLAIR MRI in the coronal plane. *B,* FLAIR MRI in the horizontal plane showing high signal intensity around the ventricles on day 18 after implantation. *C,* coronal vibratome section showing the distribution of immunostaining for CD20 (original magnification, ×3).

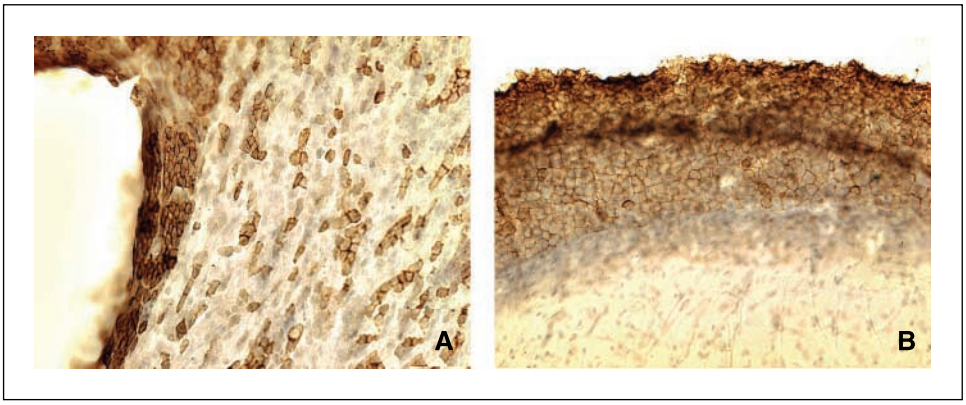

Fig. 8. Immunohistochemistry in the intraventricular CNSL model. *A,* diffuse infiltration of CD45-positive cells into brain from the left ventricle (original magnification, ×200). *B,* CD45-positive tumor cells along the meninges partially infiltrated into the parenchyma (original magnification, ×200).

time frame in the pilot study, it remains unknown whether tumor regrowth could take place.

In the radiation treatment animals, tumor volumes on histology did not match the extent of enhancement on final MRI. Tumor burden in patients also often correlates poorly with MR abnormalities in PCNSL (29, 30). New imaging methods are being developed to assess tumor response before changes in tumor volume. MRI with dynamic contrast enhancement allows noninvasive *in vivo* quantification of tumor vascular attributes such as blood volume, blood flow, mean transit time, and the permeability of the BBB and blood-tumor barriers. The dynamic MR techniques have been shown to be sensitive to changes in the BBB in animal models (31). In human studies, dynamic MRI has been used to grade gliomas, differentiate different brain tumor types, distinguish tumors from non-neoplastic lesions, and to assess brain tumor physiology (32). Changes in tumor water apparent diffusion coefficients, perfusion, and diffusion may allow early prediction of tumor responsiveness to therapy before actual tumor shrinkage (33, 34). These techniques may also be useful to assess early signs of neurotoxicity (35). The standard treatments for PCNSL cause significant neurotoxicity, particularly radiotherapy in older subjects (3, 13). Early detection of efficacy and neurotoxicity would be helpful in the clinical management of PCNSL.

We conclude that a cerebral model of human B-cell lymphoma using MC116 lymphoma cells is feasible and yields consistent and reproducible results. Further treatment approaches will be tested, including chemotherapy and monoclonal antibody–based therapies delivered i.v. (36, 37), or intra-arterially in conjunction with osmotic BBB disruption (28). Different drugs and routes of administration could be studied in this model regarding the pharmacokinetic parameters of treatments in a specific setting of CNS malignancy with a heterogeneous pattern of tumor infiltration and BBB leakage. Mechanisms of tumor cell infiltration into the brain will be further assessed, and the lymphoma infiltration pattern into the eyes and optic nerve in conjunction with the evaluation of various anti-lymphoma treatments will be evaluated as a new model of intraocular lymphoma. The intraventricular model may predominantly display the characteristics of human lymphomatous meningitis with good response to i.v. and intrathecal chemotherapy, whereas the intracerebral model could be more representative of parenchymal PCNSL, including a less pronounced response to i.v. chemotherapy. The rat CNSL models have strong potential for studying various aspects of CNSL biology, pathophysiology, and treatment.

Acknowledgments

Expert technical support by Sheila R. Taylor and Robert D. Brown was greatly appreciated.

References

1. Olson JE, Janney CA, Rao RD, et al. The continuing increase in the incidence of primary central nervous system non-Hodgkin lymphoma: a surveillance, epidemiology, and end results analysis. Cancer 2002;95:1504–10.
2. Rubenstein JL, Treseler P, O'Brien JM. Pathology and genetics of primary central nervous system and intraocular lymphoma. Hematol Oncol Clin North Am 2005;19:705–17.
3. Batchelor T, Loeffler JS. Primary CNS lymphoma. J Clin Oncol 2006;24:1281–8.
4. Grant JW, Isaacson PG. Primary central nervous system lymphoma. Brain Pathol 1992;2:97–109.
5. Schwechheimer K, Braus DF, Schwarzkopf G, Feller AC, Volk B, Muller-Hermelink HK. Polymorphous high-grade B cell lymphoma is the predominant type of spontaneous primary cerebral malignant lymphomas. Histological and immunomorphological evaluation of computed tomography-guided stereotactic brain biopsies. Am J Surg Pathol 1994;18:931–7.
6. Abrey LE, Batchelor TT, Ferreri AJ, et al. Report of an international workshop to standardize baseline evaluation and response criteria for primary CNS lymphoma. J Clin Oncol 2005;23:5034–43.
7. DeAngelis LM, Seiferheld W, Schold SC, Fisher B, Schultz CJ. Combination chemotherapy and radiotherapy for primary central nervous system lymphoma: Radiation Therapy Oncology Group Study 93–10. J Clin Oncol 2002;20:4643–8.
8. Nelson DF. Radiotherapy in the treatment of primary central nervous system lymphoma (PCNSL). J Neurooncol 1999;43:241–7.
9. Neuwelt EA, Goldman DL, Dahlborg SA, et al. Primary CNS lymphoma treated with osmotic blood-brain barrier disruption: prolonged survival and preservation of cognitive function. J Clin Oncol 1991;9:1580–90.
10. Shah GD, DeAngelis LM. Treatment of primary central nervous system lymphoma. Hematol Oncol Clin North Am 2005;19:611–27.
11. Kraemer DF, Fortin D, Doolittle ND, Neuwelt EA. Association of total dose intensity of chemotherapy in primary central nervous system lymphoma (human non-acquired immunodeficiency syndrome) and survival. Neurosurgery 2001;48:1033–40.
12. Neuwelt EA. Mechanisms of disease: the blood-brain barrier. Neurosurgery 2004;54:131–40.
13. Gavrilovic IT, Hormigo A, Yahalom J, DeAngelis LM, Abrey LE. Long-term follow-up of high-dose methotrexate-based therapy with and without whole brain irradiation for newly diagnosed primary CNS lymphoma. J Clin Oncol 2006;24:4570–4.
14. Assaf N, Hasson T, Hoch-Marchaim H, et al. An experimental model for infiltration of malignant lymphoma to the eye and brain. Virchows Arch 1997;431:459–67.
15. Schabet M, Herrlinger U. Animal models of leptomeningeal metastasis. J Neurooncol 1998;38:199–205.
16. Zubair AC, Ali SA, Rees RC, Goepel JR, Winfield DA, Goyns MH. Analysis of the colonization of unirradiated and irradiated SCID mice by human lymphoma and non-malignant lymphoid cells. Leuk Lymphoma 1996;22:463–71.
17. Saini M, Bellinzona M, Weichhold W, Samii M. A new xenograft model of primary central nervous system lymphoma. J Neurooncol 1999;43:153–60.

18. Remsen LG, McCormick CI, Sexton G, Pearse HD, Garcia R, Neuwelt EA. Decreased delivery and acute toxicity of cranial irradiation and chemotherapy given with osmotic blood-brain barrier disruption in a rodent model: the issue of sequence. Clin Cancer Res 1995;1: 731–9.

19. Hughes JA, Weckert HA, van Holst Pellekaan C, Benson EM, Dunn IS. Translocations into human chromosome 14 JH region: factors influencing downstream abortive immunoglobulin class switching. Mol Immunol 2003;40:573–83.

20. Lin CH, Kuo KT, Chuang SS, et al. Comparison of the expression and prognostic significance of differentiation markers between diffuse large B-cell lymphoma of central nervous system origin and peripheral nodal origin. Clin Cancer Res 2006;12:1152–6.

21. Kambara H, Saeki Y, Chiocca EA. Cyclophosphamide allows for *in vivo* dose reduction of a potent oncolytic virus. Cancer Res 2005;65:11255–8.

22. Roman-Goldstein SM, Goldman DL, Howieson J, Belkin R, Neuwelt EA. MR of primary CNS lymphoma in immunologically normal patients. AJNR Am J Neuroradiol 1992;13:1207–13.

23. Batchelor T, Carson K, O'Neill A, et al. Treatment of primary CNS lymphoma with methotrexate and deferred radiotherapy: a report of NABTT 96–07. J Clin Oncol 2003;21:1044–9.

24. Blay JY, Bouhour D, Carrie C, et al. The C5R protocol: a regimen of high-dose chemotherapy and radiotherapy in primary cerebral non-Hodgkin's lymphoma of patients with no known cause of immunosuppression. Blood 1995;86:2922–9.

25. Herrlinger U, Kuker W, Uhl M, et al. NOA-03 trial of high-dose methotrexate in primary central nervous system lymphoma: final report. Ann Neurol 2005;57: 843–7.

26. Omuro AM, DeAngelis LM, Yahalom J, Abrey LE. Chemoradiotherapy for primary CNS lymphoma: an intent-to-treat analysis with complete follow-up. Neurology 2005;64:69–74.

27. Dukic SF, Heurtaux T, Kaltenbach ML, Hoizey G, Laliemand A, Vistelle R. Influence of schedule of administration on methotrexate penetration in brain tumours. Eur J Cancer 2000;36:1578–84.

28. Neuwelt EA, Barnett P, McCormick CI, Remsen LG, Kroll RA, Sexton G. Differential permeability of a human brain tumor xenograft in the nude rat: the impact of tumor size and method of administration on optimizing delivery of biologically diverse agents. Clin Cancer Res 1998;4:1549–56.

29. DeAngelis LM. Cerebral lymphoma presenting as a nonenhancing lesion on computed tomographic/magnetic resonance scan. Ann Neurol 1993;33:308–11.

30. Lai R, Rosenblum MK, DeAngelis LM. Primary CNS lymphoma: a whole-brain disease? Neurology 2002; 59:1557–62.

31. Cha S, Johnson G, Wadghiri YZ, et al. Dynamic, contrast-enhanced perfusion MRI in mouse gliomas: correlation with histopathology. Magn Reson Med 2003;49:848–55.

32. Johnson G, Wetzel SG, Cha S, Babb J, Tofts PS. Measuring blood volume and vascular transfer constant from dynamic, T(2)*-weighted contrast-enhanced MRI. Magn Reson Med 2004;51:961–8.

33. Hall DE, Moffat BA, Stojanovska J, et al. Therapeutic efficacy of DTI-015 using diffusion magnetic resonance imaging as an early surrogate marker. Clin Cancer Res 2004;10:7852–9.

34. Moffat BA, Chenevert TL, Meyer CR, et al. The functional diffusion map: an imaging biomarker for the early prediction of cancer treatment outcome. Neoplasia 2006;8:259–67.

35. Fisher MJ, Khademian ZP, Simon EM, Zimmerman RA, Bilaniuk LT. Diffusion-weighted MR imaging of early methotrexate-related neurotoxicity in children. AJNR Am J Neuroradiol 2005;26:1686–9.

36. Enting RH, Demopoulos A, DeAngelis LM, Abrey LE. Salvage therapy for primary CNS lymphoma with a combination of rituximab and temozolomide. Neurology 2004;63:901–3.

37. Gordon LI, Molina A, Witzig T, et al. Durable responses after ibritumomab tiuxetan radioimmunotherapy for $CD20^+$ B-cell lymphoma: long-term follow-up of a phase 1/2 study. Blood 2004;103:4429–31.